Spiral path planning for docking of underactuated vehicles with limited FOV

Albert Sans-Muntadas*, Eleni Kelasidi*, Kristin Y. Pettersen* and Edmund Brekke*

Abstract— This paper proposes a novel approach for constructing a docking path for underwater vehicles, using a new spiral resulting of combining the Fermat and logarithmic spirals. The proposed spiral path has two properties that will help solve some of the challenges of docking autonomous underactuated vehicles (AUVs). The first property is that the spiral path reaches the entrance of the docking station without curvature, allowing a smooth transition when entering the docking station. The second is that the AUV never exceeds a certain bearing angle with respect to docking station. This last feature allows AUVs equipped with navigation sensors which have a reduced field of view (FOV), such as cameras or acoustic positioning systems, to always preserve the docking station inside the FOV. Furthermore, the paper presents an interpolation of the spiral using waypoints that are connected with segments of logarithmic spirals. This makes it possible to apply existing guidance laws to follow the docking spiral. The proposed spiral docking path has been experimentally tested using an autonomous underwater vehicle.

I. INTRODUCTION

Navigating in an environment where the global positioning system (GPS) is not available, represents one of the main challenges that autonomous underwater vehicles (AUVs) face, while operating under the surface. The lack of a GPS is often substituted by acoustic positioning and/or computer vision systems. Although these systems have proven to be able to produce accurate information, they rely in some cases on a single source of information, either because the camera tracks only a single visual landmark, or because there is only a single node of an acoustic network available. In such cases, the ability to navigate depends on the constant observation of the source (see Fig. 1) AUVs are commonly used for autonomously perform tasks like bathymetric mapping, pipeline inspection, scientific data collection, geological surveys, under ice intervention or homeland security. A common requirement which reduces the autonomy, effectiveness and feasibility of AUV operations is the need of a surface support vessel and a infrastructure that contributes to increasing the cost and to make the operational outcome more dependent on sea conditions.

Permanent underwater docking station can enable autonomous launch and recovery of AUVs, and will therefore make the AUV technology more cost effective, safer and more robust. However, underwater navigation still represents a big challenge for performing precise docking maneuvers.

A common docking scenario presented in the literature [1]–[3] describes that position data is obtained either by a single acoustic transponder attached to the docking station or by a computer vision system that identifies certain features of the docking station. In both scenarios, the ability to update the position of the vehicle relies solely on the constant observation of a single landmark. Furthermore, cameras and acoustic positioning systems are often restricted by a field of view (FOV). Preserving the landmark inside the FOV can become a determining factor in the overall success of the docking maneuver. Commonly a docking maneuver is planned trough waypoints in three stages (see the black line in Fig. 1): At the returning position Ⓡ the AUV has completed its mission and starts returning to the docking station. At this stage, the AUV is too far away for the sensors to detect the docking station, but based on previous knowledge of its position, the AUV moves in the direction where the docking station most likely is. At the starting point Ⓞ, the docking station comes into the AUV's range of vision and the vehicle starts receiving information and can accurately locate the docking station. At this point, stage two begins, and the vehicle moves to point ①, which is located at a certain distance d in front of the docking station's entrance. This distance d is prescribed according to the vehicle dynamics to give sufficient time to stabilize and reach the entrance of the docking station by following a straight trajectory ① → ⓓⓢ in stage three.

Unfortunately, depending on the navigation sensors, following a straight line from Ⓞ → ① can leave the docking station outside of the FOV [4]. While this occurs, the AUV does not receive information of the docking station position, reducing the quality of the navigation and the subsequent localization of point ①. This will affect the convergence to
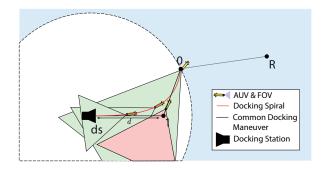
Fig. 1. Comparison of two different docking maneuvers

the final path ① → ⑮, and thus the vehicle may not recover from the combined error in position and navigation, and will thus fail to aim correctly into the docking entrance [5].

Path planning for an underactuated vehicle with restricted FOV has been studied by different authors. For instance [6] proposed a control law that guides the vehicle towards a docking station by using model predictive control preserving simultanously the FOV of the docking station. The studies in [7], [8] show that under a FOV constraint the optimal path, length-wise, to reach a given point can be described by a combination of straight lines and logarithmic spirals. However to the best knowledge of the authors, there is no description of a path that solves the challenge of reaching a final target with a given heading while simultaneously preserving the target inside the limits of the FOV. Solving the docking problem using path planning and guidance might be preferred in some cases to ensure optimality, avoid restricted regions or objects.

This paper proposes a new approach for constructing a docking path for underactuated vehicles, using a spiral result of a combination of the Fermat and logarithmic spiral's properties (represented by a red line in Fig. 1). The inherited properties of both will help solve some of the challenges of docking autonomous underactuated vehicles (AUVs). The first property, is that the bearing angle of the AUV with respect to the docking station will never exceed a certain angle, and when far from the docking station (origin) it will follow the trajectory of a logarithmic spiral. This property ensures that the docking station is always kept inside the FOV. A second property, inherited from the Fermat spiral [9], is that the proposed docking spiral reaches the entrance of the docking station without curvature and heading directly towards it, instead of at an angle, allowing a smooth transition into the docking station. Furthermore, the proposed approach has been experimentally validated by using an articulated AUV (an underwater snake robot) as testbed [10]. To control and guide the robot to the path, the paper introduces a method for interpolating the docking spiral into smaller segments of logarithmic spirals, thereby being able to use the controller described in [11] for path following. This paper is organized in the following way: Section II presents the equations of the docking spirals and analyzes its properties. Section III proposes a method to implement a guidance system for the spiral path, which includes an interpolation of logarithmic spirals in order to make it possible to use an existing guidance law to guide an underactuated AUV to converge to and follow the interpolated spiral path. Section IV presents the experimental setup followed by the presentation of the experimental results in Section V, and Section VI presents the conclusions.

II. FAMILY OF DOCKING SPIRALS

This section presents the docking spiral and the conditions that it must fulfill in order to have the preferential features for docking under restricted FOV, described in the Introduction.

Due to the nature of the spirals, this paper will follow a notation in polar coordinates (r, ϕ) to describe the spirals
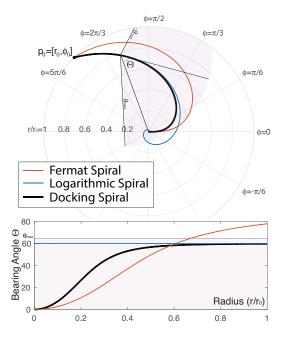

Fig. 2. Differences between the Fermat, logarithmic and docking spirals.

(see Fig. 2). Here the initial position of the vehicle is $P_0 = [r, \phi]$, and the docking station is at the origin $P_d = [0, 0]$ with its entrance facing the direction of $\phi = 0$. The bearing angle Θ is the angle between the tangent direction of the spiral and the direction of the radial vector.

The following conditions are desired to make a path useful for a docking maneuver with a underactuated vehicle with restricted FOV:

Condition 1. *The path is continuous and connects a starting point $P_0 = [r_0, \phi_0]$ with the entrance of the docking station at the origin.*

Condition 2. *The tangent of the path becomes parallel to the center line of the entrance of the docking station, and the path curvature becomes zero at the origin.*

Condition 3. *The docking station is always preserved inside the limits of the FOV, i.e. $|\Theta| \leq |\theta_{\max}|$.*

Remark 1. *Condition 2 is desired to make a smooth transition into the inside chamber of the docking station. A path with zero curvature will not have any lateral acceleration when the vehicle transits from a curve to the inside of the docking station. A straight entrance will also avoid lateral collisions with the funnel of a docking station. From a navigation perspective, Condition 3 is desired to ensure that the vehicle constantly obtains position measurements with respect to the docking station.*

The docking spiral results from the combination of two well-known spirals where a is an scaling factor:

$$\textbf{Fermat Spiral:} \quad r(\phi) = a\sqrt{\phi} \qquad (1)$$

$$\textbf{Logarithmic Spiral:} \quad r(\phi) = a e^{\frac{\phi}{\tan \theta}} \qquad (2)$$

The Fermat spiral reaches the origin with zero curvature, fulfilling conditions 1 and 2. However, when far from the

origin its bearing angle increases until being outside of the FOV. The logarithmic spiral has the property of preserving the same bearing angle with respect to its origin (see Figure 2). This implies that if the bearing angle is located inside the FOV initially, then when following the logarithmic spiral the docking station will be always kept inside the FOV, thus fulfilling Condition 3. However, the main drawback of using the logarithmic spiral is that it spirals infinitely around the origin, and thus it would not give a path where the AUV approaches the entrance of docking station following a straight line. In this paper we describe a family of spiral paths, which merges the properties of the Fermat and the logarithmic spirals, and which fulfills Conditions 1-3. We will refer to these spiral paths as **docking spirals**. The equation that describes the family of spirals is the following:

$$\textbf{Docking Spiral: } r_\lambda(\phi) = a\sqrt{\frac{e^{\frac{2\phi}{\tan(\theta)}}-e^{-\lambda\frac{2\phi}{\tan(\theta)}}}{2}} \quad (3)$$

$$\{\phi \in \mathbb{R} \mid \tfrac{\phi}{\tan(\theta)} \geq 0 \ , |\theta| \leq |\theta_{\max}|\}$$

where the angle θ is the largest bearing angle that the spiral is allowed to reach and must have the same sign as $\tan(\theta)$, the nonnegative parameter λ adjusts the transition from the logarithmic spiral to a straight line when nearing the origin (i.e. the docking station), and a is a positive parameter that scales the size of the spiral.

A. Bearing angle

The bearing angle Θ determines if the spiral path will allow to maintain the docking station inside the FOV. In this section we will show that the bearing angle of the proposed spiral never exceeds a value θ, thus we can be sure that if initially $|\theta| \leq |\theta_{\max}|$ Condition 3 holds.

Proposition 1. *The bearing angle of the docking spiral given in (3), always satisfies $|\Theta| \leq |\theta|$ for $\theta \in (-\pi/2, \pi/2)$.*

Proof. The bearing angle Θ at any point of a path described in polar coordinates, is given by

$$\tan(\Theta) = \frac{r(\phi)}{\frac{dr(\phi)}{d\phi}} \quad (4)$$

Then inserting (3) into (4) we find that:

$$\tan(\Theta) = \tan(\theta) \underbrace{\left[\frac{e^{\frac{2\phi}{\tan(\theta)}}-e^{-\frac{2\lambda\phi}{\tan(\theta)}}}{e^{\frac{2\phi}{\tan(\theta)}}+\lambda e^{-\frac{2\lambda\phi}{\tan(\theta)}}}\right]}_{\leq 1} \leq \tan(\theta) \quad (5)$$

Then, since the tangent is a class $\mathcal{K}$ function for arguments within $(-\pi/2, \pi/2)$, it follows that the bearing angle Θ is always less than or equal to the spiral's θ parameter i.e. $|\Theta| \leq |\theta|$. □

B. Zero curvature at the origin

This section shows that all the spirals of the family have zero curvature at the origin.

Proposition 2. *The curvature, κ, of the docking spiral given in (3) is zero at the origin.*

Proof. The curvature of a path described in polar coordinates is given by the following expression:

$$\kappa(r,\phi) = \frac{r^2+2\left(\frac{dr}{d\phi}\right)^2-r\left(\frac{d^2r}{d\phi^2}\right)}{\left[r^2+\left(\frac{dr}{d\phi}\right)^2\right]^{3/2}} \quad (6)$$

$$\lim_{\phi,r\to 0}\kappa(r,\phi)=0 \quad (7)$$

□

For a more concise expression, the equation of the docking spiral will be written as:

$$r(\phi) = a\sqrt{f(\phi)} \quad (8)$$

where

$$f(\phi) = \frac{e^{\frac{2\phi}{\tan(\theta)}}-e^{-\frac{2\lambda\phi}{\tan(\theta)}}}{2} \quad (9)$$

The first and second derivatives of (8) are:

$$\begin{aligned}\frac{dr}{d\phi} &= \frac{a^2}{2r}\frac{df(\phi)}{d\phi}\\ \frac{d^2r}{d^2\phi} &= \frac{a^2}{2r^2}\left[\frac{d^2f(\phi)}{d^2\phi}r-\frac{a^2}{2r}\left(\frac{df(\phi)}{d\phi}\right)^2\right]\end{aligned} \quad (10)$$

Substituting the derivatives in Equation (10) into the expression of the curvature (6) we obtain:

$$\kappa(r,\phi) = \frac{\left[6\,a^4\left(\frac{d\,f(\phi)}{d\phi}\right)^2-4\,ar^2\left(\frac{d^2\,f(\phi)}{d^2\phi}\right)+8\,r^4\right]r}{\left[a^2\left(\frac{d\,f(\phi)}{d\phi}\right)^2+4\,r^4\right]^{3/2}} \quad (11)$$

Then evaluating (10) at the origin, i.e. for $r=0, \phi=0$, we find that f' and f'' are:

$$\begin{aligned}\left.\frac{df(\phi)}{d\phi}\right|_{r,\phi=0} &= \left.\frac{\lambda e^{\frac{-2\lambda\phi}{\tan(\theta)}}+e^{\frac{2\phi}{\tan(\theta)}}}{\tan(\theta)}\right|_{\phi=0} = \frac{\lambda+1}{\tan(\theta)} > 0\\ \left.\frac{d^2\,f(\phi)}{d\phi^2}\right|_{r,\phi=0} &= \left.2\frac{-\lambda^2 e^{\frac{-2\lambda\phi}{\tan(\theta)}}+e^{\frac{2\phi}{\tan(\theta)}}}{\tan^2(\theta)}\right|_{\phi=0} = 2\frac{1-\lambda^2}{\tan^2(\theta)}\end{aligned} \quad (12)$$

From (12), it can easily be seen that the limit of the curvature exists and is zero
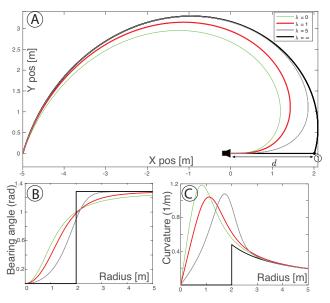

Fig. 3. The docking spiral for four different λ values

C. Special cases: $\lambda = \infty$ and $\lambda = 1$

As illustrated in Fig. 3, for the particular case of $\lambda = \infty$, the docking spiral follows exactly the logarithmic spiral until it reaches point ① (from Fig 1) and abruptly switches to a straight line that enters into the docking station. Even though the spiral $\lambda = \infty$ fulfills the Conditions 1-3, it is not a good choice due to the sudden change in the path. However since it goes trough point ①, it can serve as a reference spiral for determining the maximum bearing angle, θ, from the desired distance, d. Note that d is a prescribed distance to allow the vehicle to stabilize and follow the path to the docking station according to the dynamics of the vehicle. For the particular choice of $\lambda = 1$, the docking spiral simplifies to the following expression:

$$r_{\lambda=1}(\phi) = a\sqrt{\sinh\left(\frac{2\phi}{\tan(\theta)}\right)} \tag{13}$$

or alternatively:

$$\phi_{\lambda=1}(r) = \frac{\tan(\theta)}{2}\operatorname{arcsinh}\left(\frac{r^2}{a^2}\right) \tag{14}$$

D. Path planning with the docking spiral

This section proposes a method to adapt the equation of the docking spiral into a docking path. First, the method uses the $\lambda = \infty$ spiral to obtain the parameter θ. Note that as described in the previous section, the particular case of $\lambda = \infty$ has a segment that is a logarithmic spiral. By connecting the initial point $p_0 = [r_0, \phi_0]$ and the point $p_1 = [d, 0]$ (Point ① defined in Section I) with a logarithmic spiral, it allows us to identify the parameter θ. According to [11] the logarithmic spiral connecting the points p_0 and p_1 has the following bearing angle θ:

$$\theta = \operatorname{atan}\left(\frac{\phi_0}{\ln(r_0/d)}\right) \tag{15}$$

According to Proposition 1 if $|\theta| \leq |\theta_{\max}|$, it gives the certainty that the docking station will always be preserved inside the FOV.

Secondly, we find the value of the scaling factor a by imposing that $p_0 = [r_0, \phi_0]$ belongs to the spiral described by Equation (3):

$$a = \frac{r_0}{\sqrt{\dfrac{e^{\frac{2\phi_0}{\tan(\theta)}} - e^{-\lambda\frac{2\phi_0}{\tan(\theta)}}}{2}}} \tag{16}$$

For the particular case when $\lambda = 1$, then (16) becomes:

$$a = \frac{r_0}{\sqrt{\sinh\left(\frac{2\phi_0}{\tan(\theta)}\right)}} \tag{17}$$

The generated path, with parameters θ, a given by (15) and (16), goes from p_0 to the docking station's entrance, while keeping a bearing angle with respect to the docking station that is always smaller than θ.

III. GUIDANCE SYSTEM

In this paper we propose to use the guidance law for logarithmic spirals described in [11] in order for the vehicle to converge to and follow the spiral path. We have chosen this specific guidance law because it is shown in [11] that it preserves the docking station inside the FOV also when steering towards the path. However, we can not apply the guidance from [11] directly to the proposed docking spiral path, because it is only applicable for logarithmic spirals. To solve this, we propose an interpolation of the docking spiral path into smaller segments of logarithmic spirals.

Also this guidance method will use the $(\lambda = 1)$ docking spiral described by Equations (13-14), and the reason why this particular value of λ is chosen is because it allows us to obtain explicit expressions of both r and ϕ.

A. Interpolation of the Docking path

The path is interpolated by splitting the spiral into n segments, each connected with segments of logarithmic spirals (see Fig. 4):

$$\mathcal{P} = \{p \in \mathbb{R}^2 : p = [r(\varpi, i), \phi(\varpi, i)], \varpi \in [0,1], i \in [1...n]\} \tag{18}$$

where i is the index for each segment and ϖ is a parametrization of each point within the segment. The segments are created by $n+1$ waypoints: $p_i = [r_i, \phi_i]$, spaced with constant radius steps. This allows an explicit and compact formulation that only depends on the index i for both r_i and ϕ_i:

$$r_i = r_0\left[\frac{n-i}{n}\right] \tag{19}$$

Inserting (17) and (19) into (14) we get:

$$\phi_i = \frac{\tan(\theta)}{2}\operatorname{arcsinh}\left(\left[\frac{n-i}{n}\right]^2\sinh\left(\frac{2\phi_0}{\tan(\theta)}\right)\right) \tag{20}$$

The consecutive pair of waypoints are interpolated by logarithmic spirals, for which their constant bearing angle, found according to [11, Eq.(3)], is:

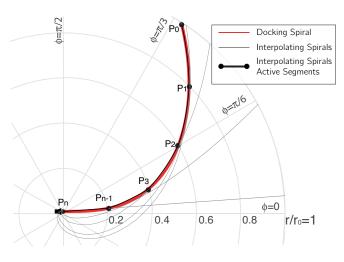$$\theta_i = \operatorname{atan}\left(\frac{\phi_i - \phi_{i-1}}{\ln(r_i/r_{i-1})}\right) \tag{21}$$

Fig. 4. Interpolation of the docking spiral: The red line shows the original docking spiral, the thick black line shows the n active segments of the logarithmic spirals used to interpolate the docking spiral and the thin lines represent the non-active regions of each logarithmic spiral.

Then the general expression of the interpolated path $\mathcal{P}$ can be obtained from substituting the waypoints from Equations (19-20) into the expression of a logarithmic spiral path found in [11, Eq.(2)]:

$$r(\varpi, i) = \frac{r_0}{n}(1 - \varpi + n - i)$$
$$\phi(\varpi, i) = \phi_{i-1} + \tan(\theta_i) \ln \left[1 - \frac{\varpi}{n-i+1} \right]$$
(22)

The length l of a logarithmic spiral between ϖ_a and ϖ_b can be calculated by integrating the curve between the two radii $r(\varpi_b, i)$, $r(\varpi_a, i)$:

$$l = \int_{r(\varpi_a, i)}^{r(\varpi_b, i)} \sqrt{1 + (rdr/d\phi)^2} dr = \frac{r(\varpi_b, i) - r(\varpi_a, i)}{\cos(\theta)}$$
(23)

Note that for a logarithmic spiral $rdr/d\phi = \tan(\theta)$. Thus the length l_i of each full segment, i.e. from $\varpi_b = 0$ to $\varpi_a = 1$ is:

$$l_i = \frac{r(0,i) - r(1,i)}{\cos(\theta_i)} = \frac{r_0}{n \cos(\theta_i)}$$
(24)

B. Serret-Frenet frame

In problems of tracking and path following, Serret-Frenet frames are often used to describe the position of the vehicle relative to a virtual particle that moves along the path (Similar approaches have been presented in [11]–[14]). The position of the particle along the path is parametrized by a distance s. However, since the proposed interpolation of the path is described by different segments of spirals, the system must first identify to which segment i_s and point ϖ_s the parametrization s maps to. Then the position of the particle is $p_s = [r(\varpi_s, i_s), \phi(\varpi_s, i_s),]$ (see Fig. 6).

To calculate ϖ_s, i_s given s we first identify i_s by finding the smallest value of the index i such that the travelled distance s is smaller than the sum of lengths of the first i segments:

$$i_s = \min i \qquad \text{s.t.} \qquad \sum_1^i l_i \geq s$$
(25)

Once the index of the current spiral i_s is known, the distance travelled for that specific segment z can be calculated by subtracting the length of the previous segments:

$$z = s - \sum_2^{i_s} l_{i_s - 1}$$
(26)

Afterwards, the traveled distance z within that segment can be found by solving Equation (23 from the waypoint $\varpi_b = 0$ to the uknown $\varpi_a = \varpi_s$:

$$z = \frac{r(0, i_s) - r(\varpi_s, i_s)}{\cos(\theta_{i_s})} = \frac{r_0 \varpi_s}{n \cos(\theta_{i_s})}$$
(27)

which makes ϖ_s:

$$\varpi_s = z/l_{i_s}$$
(28)

Once the position of the Serret-Frenet particle is known, $p_s = [r(\varpi_s, i_s), \phi(\varpi_s, i_s),]$ (Fig. 6), the position of the vehicle with respect to the path is calculated relative to the Serret-Frenet frame. The relative position of the vehicle is denoted by $x_{b/f}, y_{b/f}$ and $\psi_{b/f} \triangleq \psi - \psi_s$ is the yaw angle relative to the frame.

C. Guidance Law

In this section a brief presentation of the guidance law proposed in [11] is given, adapting it to be used for the interpolated docking spiral. The guidance has two elements: First an update law that moves the position of the Serret-Frenet frame along the path according to the update equation from [11, Eq. (13)]:

$$\dot{s} = u \cos(\psi_{b/f}) - v \sin(\psi_{b/f}) - k_x x_{b/f}$$
(29)

where u and v are the surge and sway velocities and $-k_x x_{b/f}$ acts as a restoring spring for the particle. The second element calculates the desired yaw that allows the vehicle to converge to the path while also maintaining the FOV. The desired yaw is found in [11, Eq.(14-15)].

$$\psi_d = \psi_f - \theta_i - \text{atan}\left(\frac{v}{u}\right) - \text{atan}\left(\frac{\tan(\theta_{\max})(y_{b/f} + d_{\theta_i})}{\sqrt{\Delta^2 + (y_{b/f} + d_{\theta_i})^2}}\right)$$
(30)

$$d_{\theta_i} = \Delta \tan(\theta_i)/\sqrt{\tan^2(\theta_{\max}) - \tan^2(\theta_i)}$$
(31)

which is shown to be uniformly globally asymptotically stable (UGAS) for the close-loop kinematic system. Δ is a design parameter that adjusts how sharp the vehicle should turn towards the path.

IV. EXPERIMENTAL SETUP, UNDERWATER SNAKE ROBOT AND CONTROLLERS

This section presents the experimental setup used to implement and test the docking spiral described in Section II with the interpolation and the guidance system described in Section III. Notice that the guidance is independent from the dynamics of the system, making it applicable to many different type of vehicles. For the experimental testing in this paper, we used the underwater snake robot Mamba with thrusters [15] as a test platform to validate the proposed docking approach. This is an articulated AUV with a thruster module for forward thrust, and where the joints of the robot are used instead of rudders to control its direction. In the following, the experimental setup employed for the docking and details of the underwater snake robot are briefly presented. More details can be found in [15], [16].

A. Experimental setup

The experiments were performed in the Marine Cybernetics Laboratory (MC-lab) at NTNU, Trondheim, Norway [17], in a tank of dimensions L: 40 m, H: 1.5 m and W: 6.45 m.
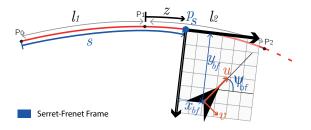

Fig. 6. Representation of the Serret-Frenet frame

Real time measurements of the position and orientation of the robot were obtained by using an underwater motion capture system from Qualisys [18] installed in the basin. The system consists of six identical cameras, that can track reflective markers under water inside a working area of dimensions 12m×1.35m×5.45m. In the tank we installed a mockup of a docking station consisting of a flat panel with a reflective circle of diameter 50 cm representing the entrance of the docking station.

The robot used for the docking experiment had a front camera with a FOV of ±30°. Below the camera the robot had mounted a template of markers that allowed the camera positioning system to accurately determine the position and heading of the robot at any time (see Fig. 5).The position of the docking station was obtained using the underwater camera system by attaching a single reflective marker on the flat panel. Afterwards, this information was used to define the docking spiral path. The position and the heading of the robot were received from an external computer to which the Qualisys system [18] was connected, and afterwards these measurements were sent through UDP in LabVIEW 2013 to another computer where the guidance and controller were implemented. The Mamba robot consists of 18 identical joint modules mounted horizontally and vertically in an alternating fashion [10], [15]. In order for the robot to move according to a strictly horizontal motion pattern, the angles for the joints with vertical rotating axis were set to zero degrees. During the experiments, the robot had a slightly positive buoyancy

and was swimming near the water surface. For more details regarding the experimental setup see [15], [16].

B. Heading Control

This subsection presents the heading controller implemented for directional control of underwater snake robots with thrusters. In previous studies, a sinusoidal motion pattern [16], [19] is commonly used, in order to provide both propulsion for underwater snake robots and for directional control. In this paper, however, we consider underwater snake robots that also are equipped with thrusters at the tail module that can provide propulsion. Results presented regarding the energy efficiency in [15] showed that it is significantly more energy efficient that USRs use the thrusters for propulsion instead of using a combination of thrusters and body undulation for propulsion. Therefore, in this paper we propose a new concept for control of underwater snake robots (USRs) with thruster. In particular, we propose that the robot joints are used for directional control, while the propulsion of the robot is only given by the thrusters. The robot thus functions as an articulated AUV, with improved maneuverability compared to rigid AUVs that use rudders for directional control. The Mamba AUV is therefore a useful platform for experimental testing in a tank of limited size, due to its excellent maneuverability properties.

There exists no previous results for such control of an articulated AUV, and we propose the following approach for heading control: Let each joint $k \in [1, \ldots, n-1]$ of the robot
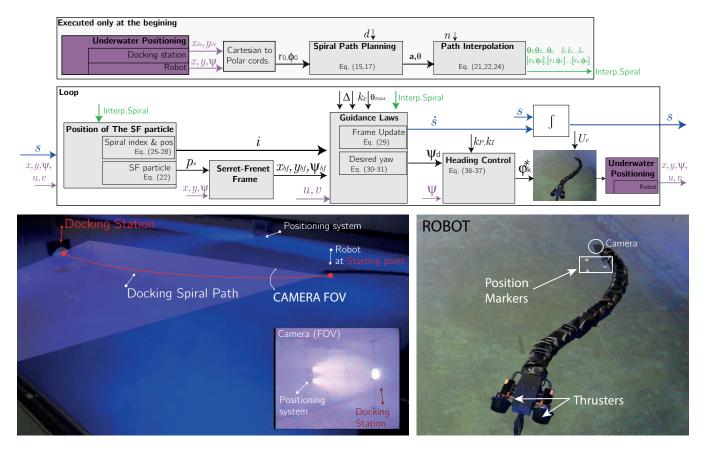

Fig. 5. The structure of the system for guidance and control, and the experimental setup

track the reference signal:

$$\varphi_k^*(t) = \varphi_0 \underbrace{\left[\frac{n-k}{n+1}\right]}_{\text{Scaling factor}} \quad (32)$$

where the scaling factor is introduced in order to achieve an increasing reference signal from head to tail. This feature is advantageous for the docking approach, since it produces smaller deflections at the head module where the camera is attached. We choose the orientation of the head angle to represent the heading, ψ, of the robot, and the reference heading ψ_d is given by the guidance law (30). The following PI heading controller is then used to make the actual heading follow its reference:

$$\varphi_0 = k_P(\psi - \psi_d) + k_I(\int \psi - \psi_d) \quad (33)$$

where $k_P > 0$ and $k_I > 0$ are control gains.

Note also that low level joint P controllers are implemented in the microcontrollers inside the modules of each link of the robot, making each joint follow the reference angles calculated by (32). In addition, a low level thruster controller is implemented, responsible for making the thruster inputs follow its references, represented by U_c in Fig. 6. The mapping from the thruster inputs to thruster forces for the underwater snake robot used in these experiments can be found in [15].

Remark 2. *In this paper, the underwater snake robot Mamba with thrusters is used as a test platform to validate the proposed docking approach. However, note that to the authors' best knowledge, investigation of docking for this kind of articulated robot has not been studied in previous literature. Therefore, the results presented in this paper not only validate the docking concept, but also present a proof of concept of using underwater snake robots for applications where docking is required.*

V. EXPERIMENTAL RESULTS

This section presents experimental validation of the proposed docking spiral described in Section II, together with the interpolation and the guidance and control system described in Sections III and IV. The results are shown in Figures 8 and 7. In Fig. 8 it is shown how the interpolation of the docking spiral through logarithmic spirals, combined with the guidance control, enables the vehicle to follow the proposed path and successfully reach the entrance of the docking station. At point A: The vehicle starts away from the path's initial point and the heading direction does not face the desired direction. From A to B the vehicle heading converges to the desired heading given by (30). The distance to the path increases during this transient period. At B the vehicle has the desired heading, and is at an offset distance from the path. Since the docking station is on the limits of the FOV, how directly the robot can steer towards the path is limited by the FOV, something which limits the convergence rate to the path. In C the vehicle reaches the path and from C to D the vehicle overshoots slightly. With better tuning we could have avoided this slight overshooting, but this was not

possible due to the limited coverage area of the underwater camera positioning system. We therefore had to give priority to fast convergence instead of a slower convergence without overshoot. After D, the vehicle manages to successfully reach the entrance of the docking station with a small offset. Note that this offset would be much smaller if the coverage area of the underwater camera system was larger, allowing us to operate in a larger area. Furthermore, the drag effects of the tether also contribute to this offset.. Fig. 7 shows how the bearing angle of the docking path, and the actual bearing angle of robot, evolves together with the FOV of the camera. As it can be seen from the series of frames, the vehicle always preserves the docking station inside the FOV. In frame 3, it can be seen how the docking station is on the limits of the FOV, and thus allows only for a small margin of steering, as we also saw for point B in Fig. 8. In frame 5 the red line seems to diverge, but this is only because the vehicle is getting close to the docking station and a small side offset represents a big bearing angle. Notice that after frame 6 the entrance of the docking station encompasses the FOV (see the angular size shaded in white) meaning that the dock is successful.

VI. CONCLUSIONS

This paper presented the development of a docking spiral path, based on the Fermat and the logarithmic spirals. The objective of the proposed spiral is to generate paths that can
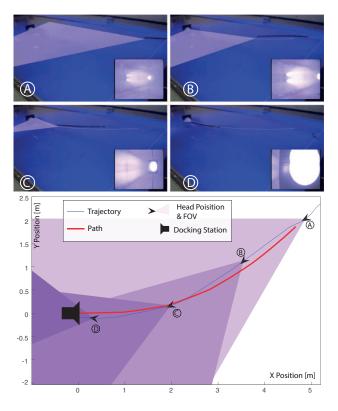

Fig. 8. The top four frames were obtained from recording the docking maneuver from one side of the tank. The images have been edited to include a virtual representation of the FOV and include the synchronized frames from the head-mounted camera. In the bottom plot, the red line represents the interpolated spiral path and the blue line displays the trajectory followed by the vehicle during the experiment.
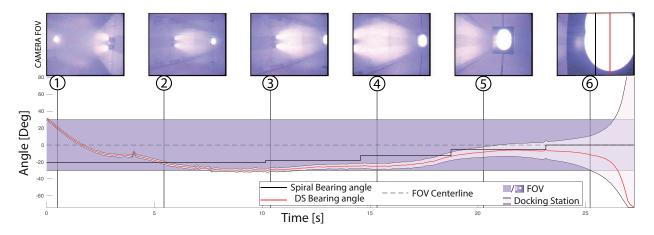
Fig. 7. On top a series of six frames obtained from the snake head camera. The plot below, which is correlated with the top images, shows in red, the bearing angle from the robot centerline to the docking station. Following the red line, the area shaded in white represents the angular size of the docking station's entrance. The black line represents the bearing angle of the docking spiral based on the position of the Serret-Frenet particle at the given time. Lastly, the area in purple represents the the FOV of the camera.

be used in applications where underactuated vehicles with restricted FOV have to reach a target, approaching it in a certain direction, while at the same time the target must be preserved inside the FOV. Additionally, this paper has proposed an interpolation of the docking spiral into segments of small logarithmic spirals, which makes it possible to implement existing guidance laws for path following of logarithmic paths.

Docking experiments have shown that the use of the docking spiral path together with an adaptation of a path following guidance control law from [11], enables an AUV to dock while preserving the docking station inside the FOV.

Future work may extend the path from 2D to 3D cases and use the observed target instead of an independent positioning system, to produce navigation data.

REFERENCES

[1] J. Evans, P. Redmond, C. Plakas, K. Hamilton, and D. Lane, "Autonomous docking for intervention-AUVs using sonar and video-based real-time 3D pose estimation," in *Proc MTS/IEEE OCEANS*, 2003.

[2] J.-Y. Park, B.-H. Jun, P.-M. Lee, and J. Oh, "Experiments on vision guided docking of an autonomous underwater vehicle using one camera," *Ocean Engineering*, vol. 36, no. 1, 2009.

[3] K. Teo, B. Goh, and O. K. Chai, "Fuzzy docking guidance using augmented navigation system on an auv," *Journal of Oceanic Engineering*, vol. 40, no. 2, 2015.

[4] R. S. McEwen, B. W. Hobson, L. McBride, and J. G. Bellingham, "Docking control system for a 54-cm-diameter (21-in) AUV," *Journal of Oceanic Engineering*, vol. 33, no. 4, 2008.

[5] A. Kukulya, A. Plueddemann, T. Austin, R. Stokey, M. Purcell, B. Allen, R. Littlefield, L. Freitag, P. Koski, E. Gallimore *et al.*, "Under-ice operations with a Remus-100 AUV in the arctic," in *Proc. Autonomous Underwater Vehicles*.

[6] S. Maniatopoulos, D. Panagou, and K. J. Kyriakopoulos, "Model predictive control for the navigation of a nonholonomic vehicle with field-of-view constraints," in *Proc. American Control Conference (ACC)*, 2013.

[7] S. Bhattacharya, R. Murrieta-Cid, and S. Hutchinson, "Optimal paths for landmark-based navigation by differential-drive vehicles with field-of-view constraints," *IEEE Transactions on Robotics*, vol. 23, no. 1, 2007.

[8] P. Salaris, L. Pallottino, S. Hutchinson, and A. Bicchi, "From optimal planning to visual servoing with limited FOV," in *Proc. International Conference on Intelligent Robots and Systems*, San Francisco, CA, 2011.

[9] A. M. Lekkas, A. R. Dahl, M. Breivik, and T. I. Fossen, "Continuous-curvature path generation using fermat's spiral," *Modeling, Identification and Control*, vol. 34, no. 4, 2013.

[10] P. Liljebäck, Ø. Stavdahl, K. Pettersen, and J. Gravdahl, "Mamba - a waterproof snake robot with tactile sensing," in *Proc International Conference on Intelligent Robots and Systems*, Chicago, IL, 2014.

[11] A. Sans-Muntadas, K. Y. Pettersen, and E. Brekke, "Vision restricted path planning and control for underactuated vehicles," in *Proc. 10th IFAC Conference on Control Applications in Marine Systems*, Trondheim, Norway.

[12] S. Moe, W. Caharija, K. Y. Pettersen, and I. Schjolberg, "Path following of underactuated marine surface vessels in the presence of unknown ocean currents," in *Proc. American Control Conference (ACC)*, Portland, OR, 2014.

[13] P. Encarnaçao and A. Pascoal, "3D path following for autonomous underwater vehicle," in *Proc. 39th IEEE Conference on Decision and Control*, Sydney, Australia, 2000.

[14] T. I. Fossen, *Handbook of marine craft hydrodynamics and motion control*. John Wiley & Sons, 2011.

[15] E. Kelasidi, K. Y. Pettersen, P. Liljebäck, and J. T. Gravdahl, "Locomotion efficiency of underwater snake robots with thrusters," in *Proc. International Symposium on Safety, Security, and Rescue Robotics (SSRR)*, Lausanne, Switzerland, 2016.

[16] E. Kelasidi, P. Liljebäck, K. Y. Pettersen, and J. T. Gravdahl, "Innovation in underwater robots: Biologically inspired swimming snake robots," *Robotics and Automation Magazin*, vol. 23, no. 1, 2016.

[17] "Marine cybernetics laboratory (MC-lab)." https://www.ntnu.edu/imt/lab/cybernetics, accessed: 2017-02-16.

[18] "Qualisys-motion." http://www.qualisys.com/, accessed: 2017-02-16.

[19] E. Kelasidi, P. Liljebäck, K. Y. Pettersen, and J. T. Gravdahl, "Integral line-of-sight guidance for path following control of underwater snake robots: Theory and experiments," *Transactions on Robotics*, 2017.